 doi:10.20944/preprints202206.0131.v1

Article

Photoplethysmogram Recording Length: Defining Minimal Length Requirement from Dynamical Characteristics

Nina Sviridova [1,2]*, Tiejun Zhao [3], Akimasa Nakano [4] and Tohru Ikeguchi [1]

[1] Faculty of Engineering, Department of Information and Computer Technology, Tokyo University of Science, 6-3-1 Niijuku, Katsushika, Tokyo 125-8585, Japan; tohru@rs.tus.ac.jp (T. I.)
[2] International Research Center for Neurointelligence, The University of Tokyo, 7-3-1 Hongo Bunkyo-ku, Tokyo, 113-0033, Japan
[3] Faculty of Agro-Food Science, Niigata Agro-Food University, 2416 Hiranedai, Tainai, Niigata, 959-2702, Japan; tiejun-zhao@nafu.ac.jp
[4] Chiba University, Innovation Management Organization, Chiba University, Kashiwano-ha Campus 6-2-1, Kashiwano-ha, Kashiwa-shi, Chiba 277-0882, Japan; anakano@chiba-u.jp
* Correspondence: nina.svr@rs.tus.ac.jp

Abstract: Photoplethysmography is a widely used technique to noninvasively assess heart rate, blood pressure, and oxygen saturation. This technique has a large potential for further applications, for example in the field of physiological and mental health monitoring. However, advanced applications of photoplethysmography have been hampered by the lack of accurate and reliable methods to analyze the characteristics of the complex nonlinear dynamics of the photoplethysmogram. Methods of nonlinear time series analysis may be used to estimate the dynamical characteristics of the photoplethysmogram but they are highly influenced by the length of the time series, which is often limited in practical photoplethysmography applications. The aim of this study was to evaluate the error in the estimation of the dynamical characteristics of the photoplethysmogram associated to the limited length of the time series. The dynamical properties were evaluated using recurrence quantification analysis, and the estimation error was computed as a function of the length of the time series. Results demonstrated that properties such as determinism and entropy can be estimated with an error lower than 1% even for short photoplethysmogram recordings. Additionally, the lower limit for the time series length to estimate the average prediction time was computed.

Keywords: photoplethysmogram; nonlinear dynamics; nonlinear time series analysis; data length assessment

1. Introduction

Cardiovascular diseases (CVD), such as heart failure, stroke, and hypertension are the leading cause of death worldwide [1]. It is recognized that accessible health monitoring and early detection of CVD can be helpful to prevent and monitor CVD. According to the World Health Organization (WHO), over three-quarters of CVD cases worldwide occur in low- and middle-income countries [1], supporting the need for accessible, affordable health monitoring systems. The photoplethysmogram (PPG) is a biological signal that has been used for decades for health monitoring in clinical settings as well as in wearable devices. Besides its main applications, which are the estimation of heart rate, respiration rate, blood pressure, and oxygen saturation, PPGs are also used for vascular assessment, arterial disease and state evaluation, sleep disorders studies, and other applications [2–5]. Moreover, a number of studies reported that the PPG is also applicable for mental health monitoring [6–11], thus PPG can be used for mental stress identification [6–8] and early detection of depression [10], which is one of the mental disorders with various social and health consequences recognized by the WHO as a leading cause of disability worldwide [12]; it is also applicable for the psychiatric patients' recovery estimation [9]. Additionally, PPG was previously applied for occupational physiological health monitoring [13–15]. In

 doi:10.20944/preprints202206.0131.v1

addition to its wide applicability for health monitoring purposes, PPG technology is also simple and inexpensive and, as such, it has a large potential for use in accessible, affordable mobile-health monitoring for prevention and early detection of disease, including CVD and mental disorders.

Common PPG applications require basic signal processing and analysis, such as contour analysis and time-frequency techniques [3,4,16–18]. Recent studies also employ neural networks and deep learning to improve the assessment or prediction of physiological states and parameters [19–21]. However, as the PPG dynamics is recognized as deterministic chaos [9,22,23], alternative complex approaches may be required for extracting accurate information on the physiological and mental health state, as follows from previous studies [9,24]. For example, nonlinear time series analysis of the PPG dynamics was applied in previous studies related to mental health monitoring [9–11].

There is a large potential for extracting information about disease and health status from the PPG dynamics by using advanced analysis methods. However, the applicability of such analysis to the PPG might be limited due to the typically high measurement noise and the presence of movement artifacts [22,23,25]. The measurement noise can be limited in clinical settings as the measurement process and settings can be strictly controlled. However, in case of measurements taken using wearable devices, both measurement noise and movement artifacts can severely hamper the extraction of information from the PPG. A common approach to address these issues is noise filtering, that is typically included in modern PPG devices and enables accurate estimation of heart rate [26]. However, filtering may alter the PPG signal and affect its nonlinear dynamics features [27]. As such, filtered signals can be efficiently used for traditional PPG applications, but they are not suitable for advanced analysis, for example nonlinear time series analysis. An alternate approach to limit the impact of noise and movement artifacts is to use only high-quality short segments of the signal. Another advantage of using short signal segments is a reduction in computational cost, the potential for a decrease in battery consumption, and enabling real-time signal processing, that is particularly important in wearable devices applications. However, short signal length may limit the applicability of nonlinear analysis and the accuracy of dynamic features estimates.

In studies involving the investigation of PPG dynamics, applied data length greatly varies, such as 2.1 s [28], 100 s [9], 2 minutes [29], 3 minutes or longer [10], 5 minutes [22,23]. To the best of our knowledge, the applicability of nonlinear analysis methods to short PPG recordings has not been systematically investigated. Among the different methods for nonlinear time series analysis, recurrence plots, which visualize the signal dynamics as a 2-dimensional binary image, and the related quantification analysis can be used to estimate the dynamical properties of time series [30,31]. Recurrence quantification analysis (RQA) was applied to the PPG to assess the effect of filtering on the PPG dynamics [27], as well as in a data-driven study on hypertension from short PPG recordings [28]. However, in the latter study, the effect of the short recordings on the nonlinear analysis was not discussed. Previous studies suggested that, differently than the majority of nonlinear time series analysis methods, RQA applied to recurrence plots is not affected by the length and drifts of the data [32]. However, at the same time, for the RQA it is generally known that longer time series provide more precise estimates of the system dynamical properties [31,32], as convergence of the RQA indexes is observed for sufficiently long time series. Overall, based on various reports [32], it appears that depending on the data under investigation meaningful results might be achieved even when the time series length is recognized as short, and let us surmise that properties of the short-recorded PPGs might be extracted by the RQA. Overall, no study so far has investigated the minimum length of a time series that can lead to reliable estimates of the dynamical properties. Stated differently, the error associated with the estimates of the dynamical properties for short PPG signals is unknown.

The aim of this paper is to assess the applicability of RQA to short PPG signals obtained from healthy human subjects in reference environment, to investigate RQA indexes that can be used to extract dynamical properties information from short PPG signals, and

Preprints (www.preprints.org) | NOT PEER-REVIEWED | Posted: 9 June 2022 doi:10.20944/preprints202206.0131.v1

to estimate the minimal length of PPG time series necessary to keep the error below an acceptable limit. As a result, it is found that by using RQA minimal time series length required for accurate dynamical properties estimation can be elucidated, thus providing a novel technique for designing data acquisition on one hand and assuring that the RQA can be applied for robust estimation of the determinism and complexity for short PPG recordings on the other.

2. Data

2.1. Photoplethysmogram

Since the PPG was introduced in 1937 [33] it was widely used for heart rate monitoring, and since then the number of its applications has expanded [2,4,18]. The PPG measurement technology mainly relies on the measurement by the photodetector of the LED light reflected or transmitted through the skin tissue. Green, red, and Near Infrared (NIR) light are the most commonly used light sources for PPG measurement. There are two main device setups depending on whether the light is transmitted or reflected. PPG device with transmission type setup schematically shown in Fig. 1 utilizes red and NIR light and is common in the hospital use; while the reflection type devices utilize green light source and are mostly applied in wearables due to the lower movement sensitivity of the green light PPGs and its flexibility in measurement location [34,35].

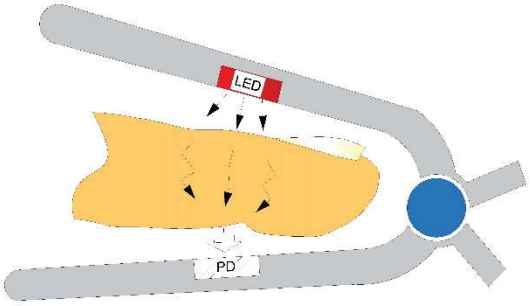

Figure 1. Conventional transmission PPG device setup.

2.2. Experimental data

In this study, the widely used NIR PPG recordings were investigated. The measurements were conducted at the Institute of Vegetable and Floriculture Science (NIVFS), NARO in 2017-2018. The experiment protocol was approved by the NIVFS ethical committee, and all participants provided informed consent prior to the experiment. Data were collected from 21–49 years old participants in sitting relaxed position inside an airconditioned room with a temperature of 25 °C. Measurements were conducted for 5 minutes and repeated twice by using a IWS920 (I.W. Technology Firm, Inc. Tokyo Devices) PPG recording device with a sampling rate 409.6Hz.

Participants were asked to evaluate their temperature and comfort perception based on category scales for comfort and temperature sensation proposed in [36]. Before the experiment, participants were asked to answer a questionnaire regarding personal history of CVDs, gender, age, presence of sickness at the time of data collection, and lifestyle habits such as smoking and sports activity. Only data from nonsmoking participants with no history of CVDs and in good health condition, who reported comfortable environmental conditions, were included in this study. As a result, a total of 30 datasets were used. An example of a 60s segment from one of the PPG recordings is shown in Fig. 2.

Preprints (www.preprints.org) | NOT PEER-REVIEWED | Posted: 9 June 2022 doi:10.20944/preprints202206.0131.v1

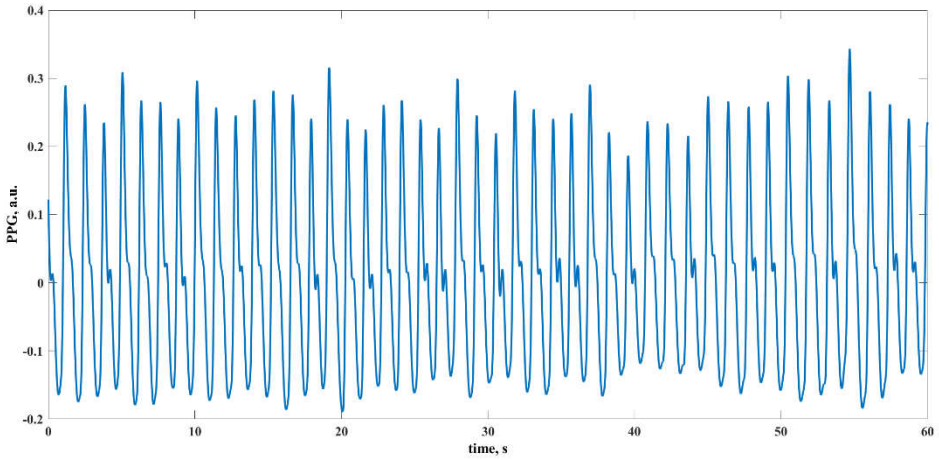

Figure 2. Example of a 60 s segment from a PPG recording.

2.3. Simulated data

As a preliminary step before evaluating the RQA results as a function of the length of the PPG segment, we assess the relationship between RQA results and segment length using the well-known chaotic Rössler model, described as follows:

$$\begin{cases} \dot{x} = -y - z, \\ \dot{y} = x + ay, \\ \dot{z} = b + z(x - c), \end{cases}$$

where $a = 0.2$, $b = 0.2$, and $c = 5.7$ [37]. The Rössler model was numerically solved using the 4th order Runge-Kutta method with sampling rate 1,000Hz. To imitate the measurement noise, additive dynamical noise was introduced. On each iteration i of the numerical solution method, noise was added to the solution x_i, using the following equation: $\tilde{x}_i = x_i + \theta\gamma_i$, where θ is the noise scaling coefficient, that varies from 0 (i.e., no noise) to 0.5 with 0.05 steps, γ_i is the i^{th} component of a fixed uniform random noise vector; and $\tilde{x}_i$ is the input of the next iteration. For computational efficiency, the resulting time series x was subsampled using a factor of five. Examples of the resulting time series obtained using the original ($\theta = 0$) and noisy ($\theta = 0.25$) x time series are shown in Fig. 3.

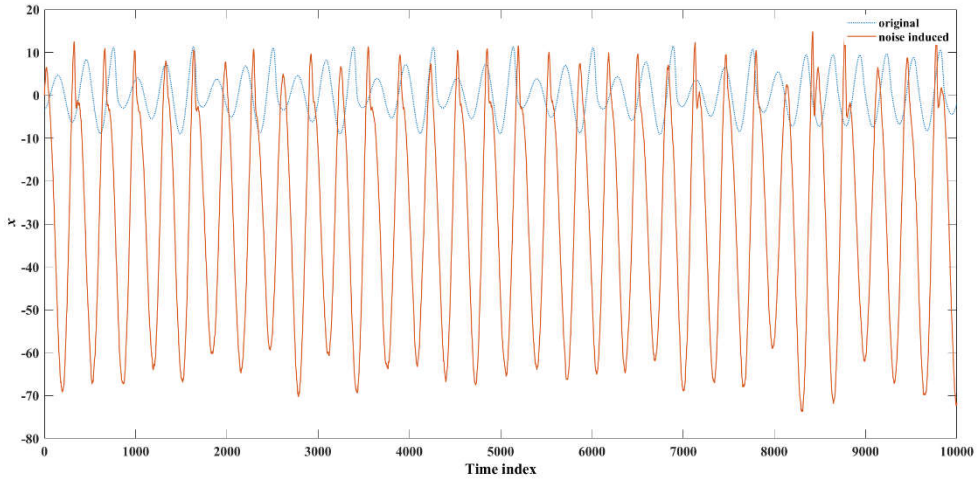

Figure 3. Examples of a segment of the original (blue dotted line) and noisy (red solid line) x time series generated using the chaotic Rössler model.

Preprints (www.preprints.org) | NOT PEER-REVIEWED | Posted: 9 June 2022 doi:10.20944/preprints202206.0131.v1

3. Analysis

3.1. Time delay reconstruction

The time-delay embedding method [38,39] is used in this study to enable nonlinear analysis, as information on the trajectory dynamics in a phase-space is needed. If a variable time series $\{x_i\}_{i=1}^{n}$ consisting of n observations is obtained, then the points of the time-delay reconstructed trajectory in an m-dimensional phase space can be calculated as [25]:

$$X_j = \left(x_j, x_{j+\tau}, x_{j+2\tau}, \dots, x_{j+(m-1)\tau}\right),$$

where $j=1,..,N$, $N = n-(m-1)\tau$, and τ is a time lag. In this study, the reconstruction dimension for the NIR PPG signal was set as $m = 4$ following [22], and the time lag was defined as the time when the signal autocorrelation falls below $1/e$ [40].

3.2. Recurrence plot

The recurrence plot (RP) visualizes the dynamics of the system as a two-dimensional binary image and is calculated using the following expression:

$$R_{i,j}(\varepsilon) = \begin{cases} 0, if \ \|X_i - X_j\| > \varepsilon \\ 1, if \ \|X_i - X_j\| < \varepsilon \end{cases}$$

where $i, j = 1,..,N$, ε is the threshold that defines the area where neighboring points of the time-delay-reconstructed trajectory are searched. If the point X_i is located within the sphere centered in X_j with radius ε, then the (i,j)-pixel is included in the RP. In this study, ε was equal to 10% of the reconstructed attractor size [32] defined by the maximal distance between attractor points: $\max_{i,j=1,..,N} \|X_i - X_j\|$.

3.3. Recurrence quantification analysis (RQA)

The RP visualizes the dynamical system as a 2-dimensional image and the displayed patterns depend on the system's dynamics. However, RP represents a qualitative descriptions of the system dynamics. RQA [31] can be applied to extract, based on the statistics of the RP, quantitative features to assess the dynamical system. In this study, the following features were estimated:

Determinism. Determinism (*DET*) is one of the most important properties of a dynamical system and defines whether the process can be expressed in the form of a system of equations. Determinism can be estimated as:

$$DET = \frac{\sum_{l=l_{min}}^{N} lP(\varepsilon, l)}{\sum_{l=1}^{N} lP(\varepsilon, l)},$$

where $P(\varepsilon, l)$ is a histogram of diagonal lines of length l defined as

$$P(\varepsilon, l) = \sum_{i,j=1}^{N} \left(1 - R_{i-1,j-1}(\varepsilon)\right)\left(1 - R_{i+1,j+1}(\varepsilon)\right)\prod_{k=0}^{l-1} R_{i+k,j+k}(\varepsilon),$$

and l_{min} is a given minimum length. Ideally, for deterministic time series, *DET* is equal to unity, whereas it is lower than one when a limited number of samples are available, when the signal includes noise, and so on. Practically, values of $DET > 0.9$ can be considered as a sign of determinism [41].

Trajectory divergence. In RQA, exponential trajectory divergence, which is an important measure of the chaotic time series, can be defined as the inverse of the length of the longest diagonal line (L_{max}) in the RP, expressed as:

$$L_{max} = \max\left(\{l_i\}_{i=1}^{N_l}\right),$$

where $N_l = \sum_{l \geq l_{min}} P(\varepsilon, l)$ is the total number of diagonal lines in the RP.

Predictability. Short-term predictability, that is the possibility to predict the future states of the signal based on the past observations for a short time window is an extremely important property, both theoretically and practically. The mean prediction time of the dynamical system can be estimated by computing the average diagonal line length (L), defined as

$$L = \frac{\sum_{l=l_{min}}^{N} lP(\varepsilon, l)}{\sum_{l=l_{min}}^{N} P(\varepsilon, l)}.$$

Preprints (www.preprints.org) | NOT PEER-REVIEWED | Posted: 9 June 2022 doi:10.20944/preprints202206.0131.v1

Complexity. Entropy (*ENTR*) is frequently used in applied studies of RQA. *ENTR* estimates the complexity of the RP with respect to the diagonal lines and can be calculated as:

$$ENTR = -\sum_{l=l_{min}}^{N} p(l)\ln p(l),$$

where $p(l) = P(\varepsilon, l)/N_l$ is the estimated probability to find a diagonal line of length l in the RP, and N_l is the number of diagonal lines.

3.4. Error estimation

In this study, the lower limit of the length of the time series was determined by considering the average time required for the original time-delay-reconstructed trajectory to complete one turn on the time-delay-reconstructed attractor, hereinafter average cycle. Specifically, the lower limit of the length of the time series was set as the time required to complete 3-5 average cycles to ensure the presence of at least one separated cycle fragment of trajectory in the neighborhood, depending on the density of the reconstructed attractor trajectories. The length of the time series (T) assumed to lead to accurate estimates of the RQA features defined in Section 3.3 was defined as over 100 average turns of the trajectory on the reconstructed attractor. A set of RPs were computed and RQA was performed for varying length of the time series. For each RQA feature S, the relative error E_l associated with the estimate of S using a time series of length l with respect to the accurate measure obtained using a time series of length T was calculated as follows [42]:

$$E_l = \frac{|S_l - S_T|}{S_T} \times 100\%.$$

4. Results

4.1. Rössler system

First, for the time series x of the original and noisy Rössler system defined in Section 2.3 the time-delay reconstructed attractor was obtained. Figure 4 (a) and (b) show the obtained attractors for the original and noisy time series, respectively. Then, the set of RPs was calculated for varying length of the segments of the obtained trajectory of the attractor. The length of the time series was varied from 1500 data points (5 average cycles) to 50000 data points (168 average cycles). For each length, 100 different segments were chosen on the attractor and corresponding RPs were calculated. Figure 4 (c) and (d) show the RPs corresponding to a length of 10000-points for the original and noisy trajectories shown in Fig. 4 (a) and (b), respectively.

Preprints (www.preprints.org) | NOT PEER-REVIEWED | Posted: 9 June 2022 doi:10.20944/preprints202206.0131.v1

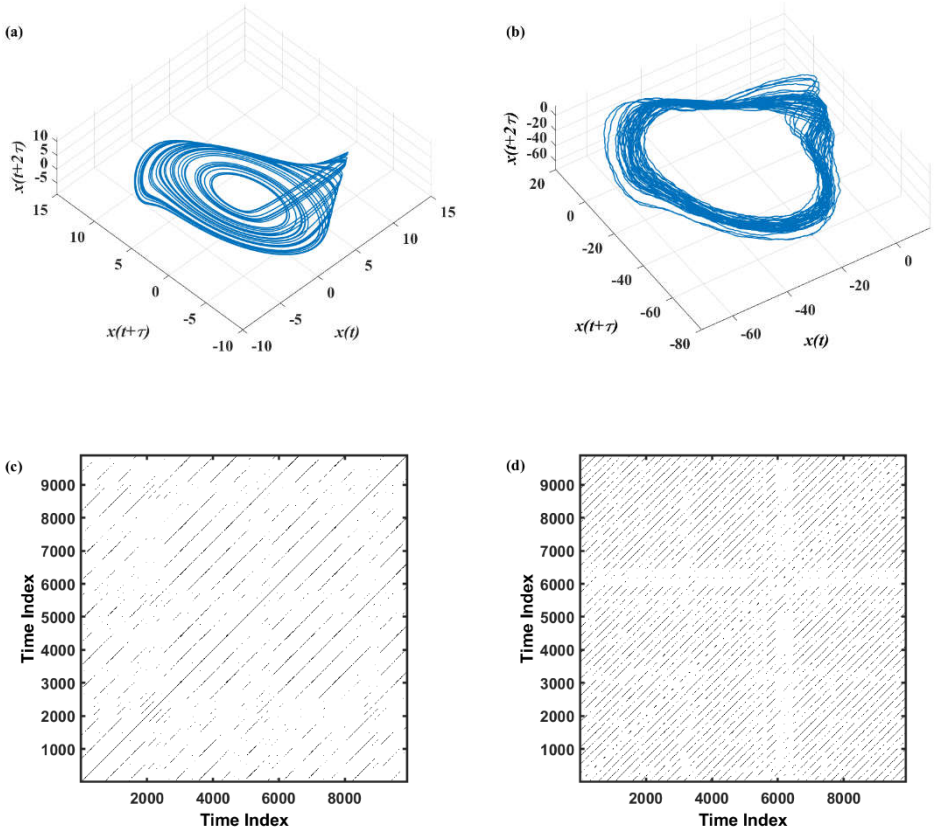

Figure 4. Reconstructed attractors from x time series of (a) original (θ = 0) and (b) noisy (θ = 0.25) Rössler system's and the resulting RPs (panels (c) and (d), respectively).

Figure 5 shows the relative error of *DET* (a), L_{max} (b), *L* (c), and *ENTR* (d) as a function of noise level (θ) and time series length, as averaged over 100 segments. Table 1 shows four calculated RQA measures reference values for three levels of noise. Table 2 shows the time series length corresponding to relative errors equal to 5% and 1% for three different noise levels. A relative error lower than or equal to 1% is considered acceptable, therefore the corresponding length can be used as a benchmark for the minimal length of the time series. Figure 6 shows detailed information of the length of the time series associated to relative error below 5% and 1% for the four RQA features here computed.

Preprints (www.preprints.org) | NOT PEER-REVIEWED | Posted: 9 June 2022 doi:10.20944/preprints202206.0131.v1

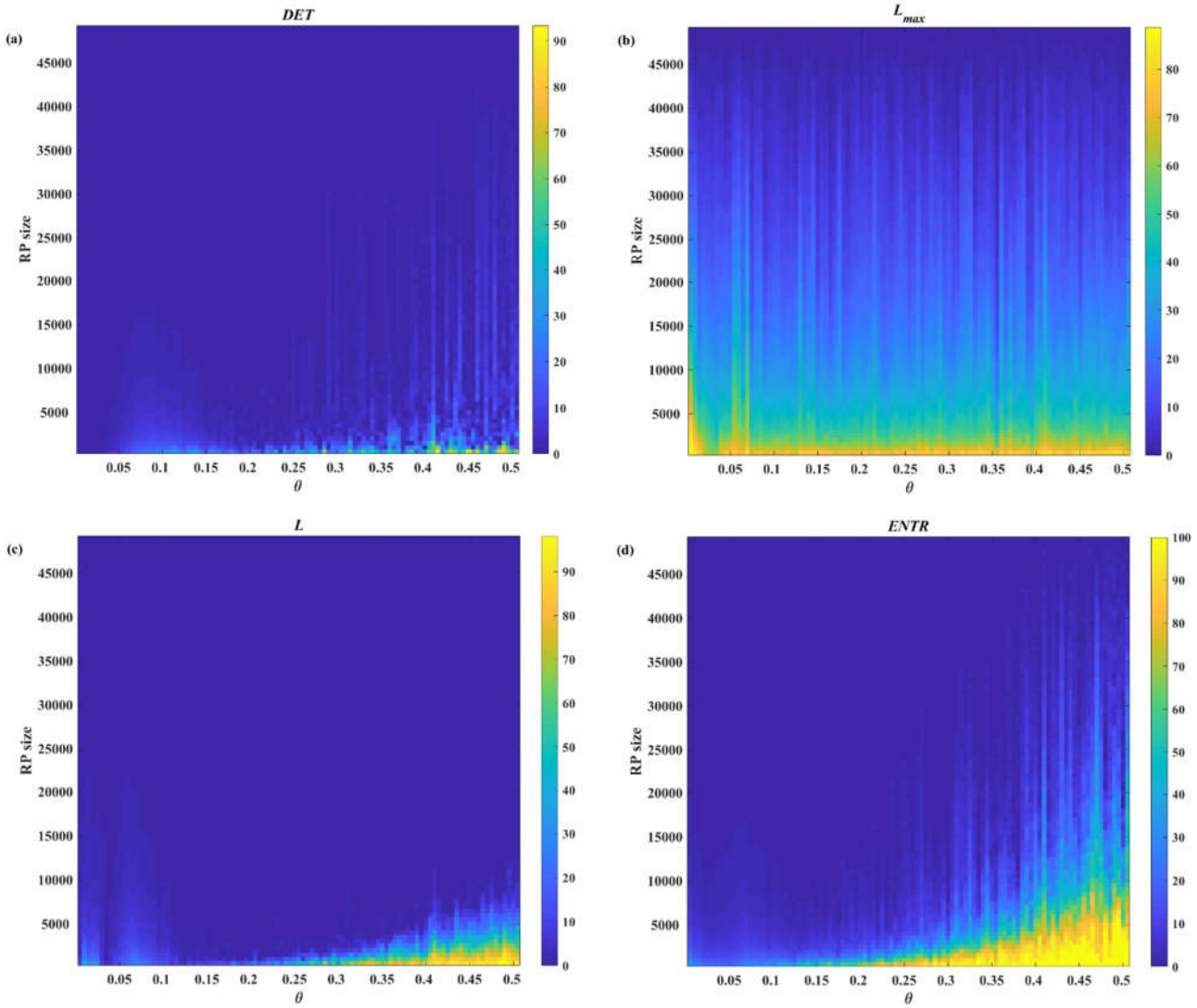

Figure 5. Relative error of the RQA features estimates as a function of length and noise level of Rössler time series: (a) determinism, (b) maximal diagonal line length, (c) average diagonal line length, and (d) entropy.

Table 1. Values of determinism, maximal diagonal line length, average diagonal line length, and entropy obtained for long Rössler's x time series for three different noise levels.

Noise level, θ	*DET*	L_{max}	*L*	*ENTR*
0	0.9992	3763.9	60.4329	4.6079
0.245	0.4138	7.52	2.3379	0.7544
0.5	0.0910	3.24	2.0455	0.1765

Preprints (www.preprints.org) | NOT PEER-REVIEWED | Posted: 9 June 2022 doi:10.20944/preprints202206.0131.v1

Table 2. Time series length corresponding to relative errors equal to 5% and 1% in the estimates of determinism, maximal diagonal line length, average diagonal line length, and entropy for three different noise levels of the Rössler time series. The values highlighted indicate the lower limit of the length of the time series required for accurately estimating the four features.

Noise level, θ	E_l	*DET*	L_{max}	*L*	*ENTR*
0	5%	1500	46000	4000	10500
	1%	1500	48500	16000	26000
0.245	5%	3000	36500	2500	7500
	1%	17000	46000	3500	30000
0.5	5%	5000	41500	11000	42000
	1%	7000	47000	13500	43500

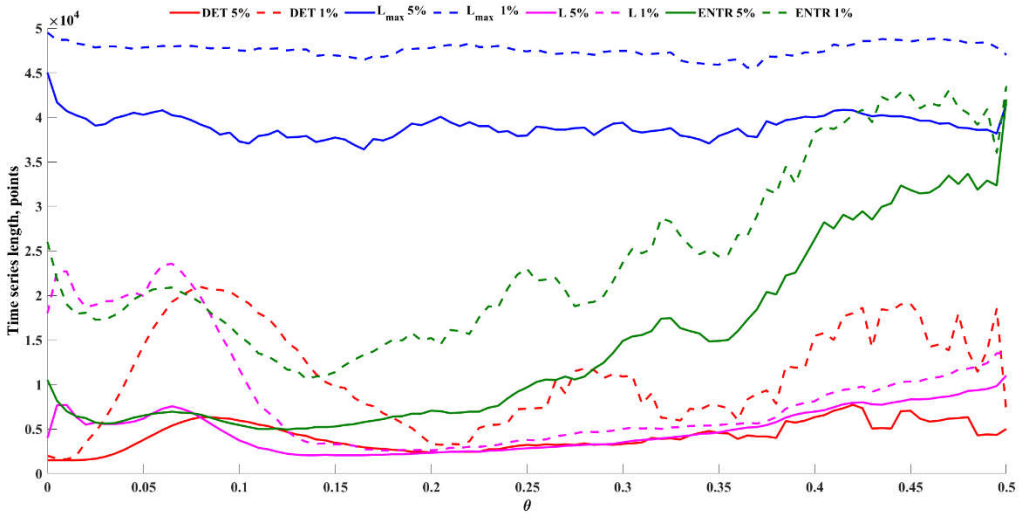

Figure 6. Length of the Rössler time series as a function of the noise level corresponding to a relative error equal to 5% (solid line) and 1% (dashed line) in the estimation of the determinism (red), maximal diagonal line length (blue), average diagonal line length (magenta), and entropy (green).

4.2. Photoplethysmogram

Similarly to the Rössler system case described in Section 4.1, for each measured PPG time series, the time-delay-reconstructed attractor was computed. Then, for each reconstructed attractor, the set of RPs corresponding to the segment of the trajectory with length from 3 to 152 average cycles was calculated (i.e., 2.4 s to 122 s). The length of the average cycle was chosen taking into account the physiological properties of the PPG signal, specifically the average cycle was set at 0.8 s, that is the average duration of the heartbeat cycle in healthy human subjects. Then, the RQA measures were estimated from the obtained RPs. An example of the time-delay-reconstructed attractor and the corresponding RP obtained from a 24.4 s-long PPG segment is shown in Fig. 7. Figure 8 shows the average relative error of the RQA features estimates as a function of the length of the time series. Table 3 summarizes the lower limits for the length of the time series length that provide RQA features estimates with relative error below 5% and 1%, and the reference RQA values.

Preprints (www.preprints.org) | NOT PEER-REVIEWED | Posted: 9 June 2022 doi:10.20944/preprints202206.0131.v1

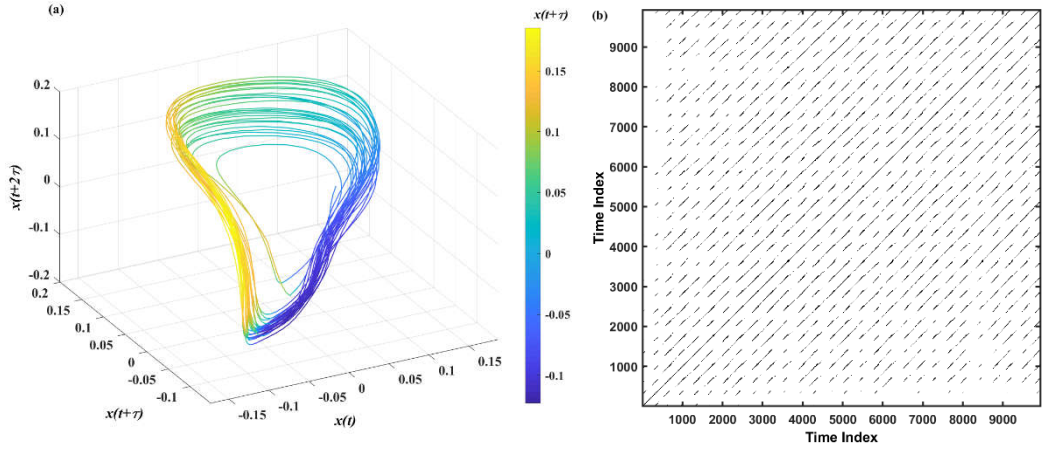

Figure 7. An example of (a) time-delay-reconstructed attractor and (b) the resulting RP obtained from one of the PPGs recorded in this study.

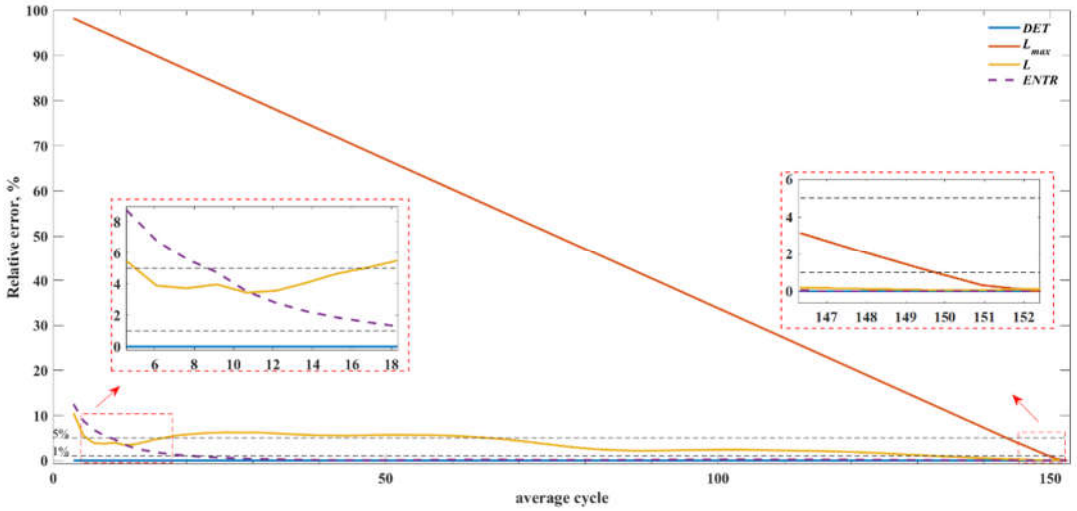

Figure 8. Relative error of the RQA features estimates as a function of the length of the time series.

Table 3. Average values of the length of the time series corresponding to relative error below 5% and 1%, and the reference RQA values.

	Lower time series length limit, points		Reference RQA values
	E_l, 5%	E_l, 1%	
DET	1000	1000	0.998
L_{max}	47500	49120	48859
L	21500	43000	144.38
ENTR	2500	7000	5.73

5. Discussion

The main aim of this preliminary study was to evaluate the error associated with RQA features estimates as a function of the length of the PPG time series and to identify recommended limits for the length of PPG recordings in order to keep the error below acceptable levels (e.g., 1%). In this study, PPG recordings measured in healthy individuals sitting comfortably in a relaxed position were used.

In addition, the relative error of RQA features estimates was assessed for original and noisy time series generated using the chaotic Rössler model. The distributions of the relative error associated with the estimates of *DET*, L_{max}, *L*, and *ENTR* shown in Fig. 5 (a)-(d) indicate specific patterns associated with the different RQA features. As seen in Fig. 5 (a),

Preprints (www.preprints.org) | NOT PEER-REVIEWED | Posted: 9 June 2022 doi:10.20944/preprints202206.0131.v1

accurate estimates of determinism can be achieved even for very short time series (e.g., 1500 points). The lowest acceptable length of the time series increases with increasing noise as shown in Fig 5 (a), Table 2, and Fig. 6, but *DET* remains the feature requiring the shortest time series length among the RQA features addressed in this study. It is to note that with high levels of added noise, the time series cannot be considered deterministic as *DET* decreases significantly below 0.9 (Table 1).

The analysis of the error associated with the L_{max} showed that accurate estimates of this feature, that is the inverse of the divergence, cannot be achieved for short time series (Fig. 5 (b), Fig. 6) as L_{max} requires long time series, i.e. longer than 48500 points, for obtaining errors below 1%. It is to be noticed that the average L_{max} value for original data (i. e., 3763.9 points, Table 1) is significantly shorter than the used maximal time series length, nevertheless, resulting lower limit for time series length is compatible with the maximal time series length used. Figures 5(b) and 6 and Table 2 also clearly demonstrated that in the absence of noise the lowest acceptable length of the time series is higher than that observed with noisy data, due to the fact that the presence of noise significantly shortens the length of the maximal diagonal lines (Table 1).

The error patterns observed for *L* (Fig. 5 (c)), that is an important measure characterizing the average prediction time, show that the lowest acceptable length of the time series is longer for original data, and it decreases with increasing noise (in the range 0.065-0.15), due shorter diagonal lines (Table 1), while the determinism is preserved, and then it steadily increases again for higher noise. A similar pattern was observed for *ENTR* (Fig. 5 (d), Fig. 6), that quantifies time series complexity, (Fig. 5 (d)), suggesting that the observed trend attributed to high levels of noise disrupting data determinism (Table 1).

Overall, the results observed for the original and noisy Rössler model time series, suggest that determinism can be accurately estimated even for short time series and that, if the time series is deterministic (i.e., if noise is sufficiently low), *L* and *ENTR* can be estimated accurately for substantially shorter time series than the reference length (i.e., 50000). Specifically, for $\theta < 0.2$ time series with length above 25000 points or 85 average cycles provide acceptable estimates if an error limit equal to 1% is set, and shorter time series could be used if higher errors are accepted (e.g., 10000 points for 5% error limit).

The PPG signal inevitably contains a certain amount of measurement noise. The results shown in Fig. 8 and Table 3 show that, similarly to the noisy Rössler model, *DET* can be correctly estimated even for very short lengths of PPG time series, specifically 1000 points (3.05 average cycles or 2.44 s). The *ENTR* can be evaluated with error below 1% for 7000 points (21.35 average cycles or 17.08 s) time series. For the estimates of *L* and L_{max}, longer time series are required to reach error below 1%, specifically 43000 (131.15 average cycles or 104.92 s) and 49120 (149.75 average cycles or 119.8 s), respectively. However, for the L_{max} lower limit of the time series almost reaches the maximal time series length, and the actual L_{max} value, unlike the results of the simulated data, is comparable with the maximal time series length, thus making it inapplicable for short recordings of investigated PPG type.

The observed relationships between the error associated with each RQA feature estimate and the signal length, as reported in Fig. 8, can be used to predict the average error level in practical applications in which only limited segments of the PPG are available. For example, if a 2.5 s PPG time series is available, accurate estimates of determinism can be expected and the estimates of *ENTR* will be associated with an error equal to approximately 12%, whereas for 3.8 s PPG time series the estimates of *ENTR* are associated with an average error lower than 5%, that may be a sufficiently low error in practical applications.

It is to notice that the results presented in this study apply to the transmission type NIR PPG signals collected in the reference environment, therefore further studies are required to confirm limited time-series length related error in dynamical properties estimation by RQA for other types of PPG signals as well as for different experimental settings. Additionally, the significantly different sampling rate of the signal may affect

 doi:10.20944/preprints202206.0131.v1

demonstrated results; however, it is expected that these results are applicable to the PPGs with comparable sampling rates.

6. Conclusion

The results of this study can support a deeper understanding of the accuracy of the dynamic features estimated from experimental PPG time series of limited length in real-world applications, for example health monitoring using wearable devices. Specifically, this study investigated the effect of the length of the time series on the accuracy of the estimates of the RQA features estimated from NIR light-based PPG signals. As a result, minimum requirements for the length of the PPG time series needed to obtain sufficiently accurate estimates of the dynamical properties of the signal could be defined, as relevant to practical studies and experiment design.

Author Contributions: Conceptualization, N.S. and T.I; methodology, N.S.; software, N.S.; validation, N.S. and T.I.; formal analysis, N.S.; investigation, N.S., T.Z, and A.N.; resources, N.S., T.Z, and A.N.; data curation, N.S., T.Z, and A.N.; writing—original draft preparation, N.S.; writing—review and editing, N.S., T.Z, A.N., and T.I.; visualization, N.S and T.Z.; supervision, N.S., T.Z, A.N., and T.I.; project administration, N.S., T.Z. and A.N.; funding acquisition, N.S. and T.I. All authors have read and agreed to the published version of the manuscript.

Funding: This work was partially supported by JSPS KAKENHI Grant Number JP19K14589, JP20H00596 and JP21H03514.

Institutional Review Board Statement: The study was conducted in accordance with the Declaration of Helsinki, and approved by Ethics Committee of Institute of Vegetable and Floriculture Science of National Agriculture and Food Research Organization (NARO) (protocol acceptance number 2, date of approval November 2nd 2017).

Informed Consent Statement: Informed consent was obtained from all subjects involved in the study.

Data Availability Statement: Not applicable.

Conflicts of Interest: The authors declare no conflict of interest.

References

1. Cardiovascular Diseases (CVDs) Available online: https://www.who.int/news-room/fact-sheets/detail/cardiovascular-diseases-(cvds) (accessed on 5 June 2022).
2. Allen, J. Photoplethysmography and Its Application in Clinical Physiological Measurement. *Physiol. Meas.* **2007**, *28*, R1–R39, doi:10.1088/0967-3334/28/3/R01.
3. Elgendi, M. *PPG Signal Analysis: An Introduction Using MATLAB*; CRC Press: Boca Raton, 2020; ISBN 978-0-429-44958-1.
4. Kyriacou, P.A. Introduction to Photoplethysmography. In *Photoplethysmography*; Allen, J., Kyriacou, P., Eds.; Academic Press, 2022; pp. 1–16 ISBN 978-0-12-823374-0.
5. Tamura, T. Current Progress of Photoplethysmography and SPO2 for Health Monitoring. *Biomed. Eng. Lett.* **2019**, *9*, 21–36, doi:10.1007/s13534-019-00097-w.
6. Celka, P.; Charlton, P.H.; Farukh, B.; Chowienczyk, P.; Alastruey, J. Influence of Mental Stress on the Pulse Wave Features of Photoplethysmograms. *Healthc Technol Lett* **2019**, *7*, 7–12, doi:10.1049/htl.2019.0001.
7. Charlton, P.H.; Celka, P.; Farukh, B.; Chowienczyk, P.; Alastruey, J. Assessing Mental Stress from the Photoplethysmogram: A Numerical Study. *Physiol. Meas.* **2018**, *39*, 054001, doi:10.1088/1361-6579/aabe6a.
8. Correia, B.; Dias, N.; Costa, P.; Pêgo, J.M. Validation of a Wireless Bluetooth Photoplethysmography Sensor Used on the Earlobe for Monitoring Heart Rate Variability Features during a Stress-Inducing Mental Task in Healthy Individuals. *Sensors* **2020**, *20*, 3905, doi:10.3390/s20143905.
9. Tsuda, I.; Tahara, T.; Iwanaga, H. Chaotic Pulsation in Human Capillary Vessels and Its Dependence on Mental and Physical Conditions. *International Journal of Bifurcation and Chaos* **1992**, *2*, 313–324, doi:10.1142/s0218127492000318.
10. Pham, T.D.; Thang, T.C.; Oyama-Higa, M.; Sugiyama, M. Mental-Disorder Detection Using Chaos and Nonlinear Dynamical Analysis of Photoplethysmographic Signals. *Chaos, Solitons & Fractals* **2013**, *51*, 64–74, doi:10.1016/j.chaos.2013.03.010.
11. Sumida, T.; Arimitu, Y.; Tahara, T.; Iwanaga, H. Mental Conditions Reflected by the Chaos of Pulsation in Capillary Vessels. *Int. J. Bifurcation Chaos* **2000**, *10*, 2245–2255, doi:10.1142/s0218127400001407.
12. Depression Available online: https://www.who.int/news-room/fact-sheets/detail/depression (accessed on 6 June 2022).
13. Sviridova, N.; Sakai, K. Application of Photoplethysmogram for Detecting Physiological Effects of Tractor Noise. *Engineering in Agriculture, Environment and Food* **2015**, *8*, 313–317, doi:10.1016/j.eaef.2015.03.006.

14. Hwang, S.; Seo, J.; Jebelli, H.; Lee, S. Feasibility Analysis of Heart Rate Monitoring of Construction Workers Using a Photoplethysmography (PPG) Sensor Embedded in a Wristband-Type Activity Tracker. *Automation in Construction* **2016**, *71*, 372–381, doi:10.1016/j.autcon.2016.08.029.
15. Bradke, B.S.; Miller, T.A.; Everman, B. Photoplethysmography behind the Ear Outperforms Electrocardiogram for Cardiovascular Monitoring in Dynamic Environments. *Sensors* **2021**, *21*, 4543, doi:10.3390/s21134543.
16. Elgendi, M. On the Analysis of Fingertip Photoplethysmogram Signals. *Curr Cardiol Rev* **2012**, *8*, 14–25, doi:10.2174/157340312801215782.
17. Millasseau, S.C.; Ritter, J.M.; Takazawa, K.; Chowienczyk, P.J. Contour Analysis of the Photoplethysmographic Pulse Measured at the Finger. *Journal of Hypertension* **2006**, *24*, 1449–1456, doi:10.1097/01.hjh.0000239277.05068.87.
18. Bhat, S.; Adam, M.; Hagiwara, Y.; Ng, E.Y.K. The Biophysical Parameter Measurements from Ppg Signal. *J. Mech. Med. Biol.* **2017**, *17*, 1740005, doi:10.1142/S021951941740005X.
19. Kumar, A.K.; Ritam, M.; Han, L.; Guo, S.; Chandra, R. Deep Learning for Predicting Respiratory Rate from Biosignals. *Computers in Biology and Medicine* **2022**, *144*, 105338, doi:10.1016/j.compbiomed.2022.105338.
20. Rong, M.; Li, K. A Multi-Type Features Fusion Neural Network for Blood Pressure Prediction Based on Photoplethysmography. *Biomedical Signal Processing and Control* **2021**, *68*, 102772, doi:10.1016/j.bspc.2021.102772.
21. Kim, J.W.; Choi, S.-W. Normalization of Photoplethysmography Using Deep Neural Networks for Individual and Group Comparison. *Sci Rep* **2022**, *12*, 3133, doi:10.1038/s41598-022-07107-5.
22. Sviridova, N.; Sakai, K. Human Photoplethysmogram: New Insight into Chaotic Characteristics. *Chaos, Solitons & Fractals* **2015**, *77*, 53–63, doi:10.1016/j.chaos.2015.05.005.
23. Sviridova, N.; Zhao, T.; Aihara, K.; Nakamura, K.; Nakano, A. Photoplethysmogram at Green Light: Where Does Chaos Arise From? *Chaos, Solitons & Fractals* **2018**, *116*, 157–165, doi:10.1016/j.chaos.2018.09.016.
24. Kaneko, K.; Tsuda, I. *Complex Systems: Chaos and Beyond*; Springer: Berlin, Heidelberg, 2001; ISBN 978-3-642-63132-0.
25. Shelhamer, M. *Nonlinear Dynamics in Physiology: A State-Space Approach*; WORLD SCIENTIFIC, 2006; ISBN 978-981-270-029-2.
26. Liang, Y.; Elgendi, M.; Chen, Z.; Ward, R. An Optimal Filter for Short Photoplethysmogram Signals. *Sci Data* **2018**, *5*, 180076, doi:10.1038/sdata.2018.76.
27. Sviridova, N. Detection of Preprocessing-Induced Changes in Chaotic Characteristics of Human Photoplethysmogram. In Proceedings of the Proceedings of Int'l Symposium on Nonlinear Theory and its Applications 2019; 2019; pp. 540–543.
28. Sviridova, N.; Ikeguchi, Tohru Application of Recurrence Quantification Analysis to Hypertension Photoplethysmograms. In Proceedings of the Proceedings of Int'l Symposium on Nonlinear Theory and its Applications 2020; 2020; pp. 56–58.
29. Sato, S.; Miao, T.; Oyama-Higa, M. Studies on Five Senses Treatment. In *Knowledge-Based Systems in Biomedicine and Computational Life Science*; Pham, T.D., Jain, L.C., Eds.; Studies in Computational Intelligence; Springer: Berlin, Heidelberg, 2013; pp. 155–175 ISBN 978-3-642-33015-5.
30. Webber, C.L.; Zbilut, J.P. Dynamical Assessment of Physiological Systems and States Using Recurrence Plot Strategies. *Journal of Applied Physiology* **1994**, *76*, 965–973, doi:10.1152/jappl.1994.76.2.965.
31. Marwan, N.; Carmen Romano, M.; Thiel, M.; Kurths, J. Recurrence Plots for the Analysis of Complex Systems. *Physics Reports* **2007**, *438*, 237–329, doi:10/fbbwkj.
32. Marwan, N. How to Avoid Potential Pitfalls in Recurrence Plot Based Data Analysis. *Int. J. Bifurcation Chaos* **2011**, *21*, 1003–1017, doi:10.1142/s0218127411029008.
33. Hertzman, A.B. Photoelectric Plethysmography of the Fingers and Toes in Man. *Proceedings of the Society for Experimental Biology and Medicine* **1937**, *37*, 529–534, doi:10.3181/00379727-37-9630.
34. Maeda, Y.; Sekine, M.; Tamura, T.; Suzuki, T.; Kameyama, K. Performance Evaluation of Green Photoplethysmography. *Journal of Life Support Engineering* **2007**, *19*, 183–183, doi:10.5136/lifesupport.19.Supplement_183.
35. Maeda, Y.; Sekine, M.; Tamura, T. The Advantages of Wearable Green Reflected Photoplethysmography. *J Med Syst* **2011**, *35*, 829–834, doi:10.1007/s10916-010-9506-z.
36. Gagge, A.P.; Stolwijk, J.A.J.; Hardy, J.D. Comfort and Thermal Sensations and Associated Physiological Responses at Various Ambient Temperatures. *Environmental Research* **1967**, *1*, 1–20, doi:10.1016/0013-9351(67)90002-3.
37. Rössler, O.E. An Equation for Continuous Chaos. *Physics Letters A* **1976**, *57*, 397–398, doi:10.1016/0375-9601(76)90101-8.
38. Takens, F. Detecting Strange Attractors in Turbulence. In Proceedings of the Dynamical Systems and Turbulence, Warwick 1980; Rand, D., Young, L.-S., Eds.; Springer: Berlin, Heidelberg, 1981; pp. 366–381.
39. Sauer, T.; Yorke, J.A.; Casdagli, M. Embedology. *J Stat Phys* **1991**, *65*, 579–616, doi:10.1007/bf01053745.
40. Albano, A.M.; Muench, J.; Schwartz, C.; Mees, A.I.; Rapp, P.E. Singular-Value Decomposition and the Grassberger-Procaccia Algorithm. *Phys. Rev. A* **1988**, *38*, 3017–3026, doi:10.1103/physreva.38.3017.
41. Thiel, M.; Romano, M.C.; Kurths, J.; Meucci, R.; Allaria, E.; Arecchi, F.T. Influence of Observational Noise on the Recurrence Quantification Analysis. *Physica D: Nonlinear Phenomena* **2002**, *171*, 138–152, doi:10/dprjhd.
42. Anton, H.; Bivens, I.; Davis, S. *Calculus.*; 7th ed. / Howard Anton, Irl Bivens, Stephen Davis.; John Wiley & Sons: New York, 2002; ISBN 978-0-471-43312-5.